Control Architecture based on FPGA for a Renewable Energy System

António Martins, Vitor Morais, Mário Ferreira, Adriano Carvalho
Faculty of Engineering - University of Porto
Rua Dr Roberto Frias, s/n 4200-465, Porto, Portugal
email: {ajm, vitormorais, mnaia, asc}@fe.up.pt

***Abstract*—Renewable energy systems require real-time and distributed control architectures for achieving high performance levels both in steady-state operation and in transient conditions. Thus, command, control, monitoring and communication functions must be implemented using platforms like uCs, DSPs, or FPGAs. Structuring all the architecture is of fundamental importance when the system contains several and quite different energy sources and is designed to operate in some degraded modes. In this paper it is discussed and presented the design and implementation of a global control and monitoring architecture for a renewable energy system including wind and photovoltaic energy, battery storage and electric grid connection.**

***Index Terms*—AC-DC converter, Digital control, FPGA, Renewable energy, Sensorless control.**

I. Introduction

Distributed generating systems, electric vehicles, FACTS devices, micro-grids, multilevel converters, renewable energy systems (among others) are complex power electronics based systems requiring appropriate real-time controllers, supervisors and communication channels, [1]. High reliability figures, fault tolerance capability and fast processing are essential features required by such systems. Usually, these systems include more than one renewable energy source and, often, are accompanied by energy storage, normally by means of battery packs. Frequently, the power electronics converters above referred are connected to the electric grid and, therefore, require a current control loop that is deterministic, predictable and fast enough to avoid transient overshoots in the output current even in fast transient conditions, [2], [3]. This specific requirement cannot be matched with common microprocessors; they do not have enough processing capability. A possible solution can be obtained by using an FPGA, running several processes in parallel and using highly robust state machines, [4], [5].

To implement efficient real-time industrial control systems, designers have the choice between two main types of digital device technologies. The first category is based on a pure software platform and the associated devices are microcontrollers (uC) and Digital Signal Processor (DSP) controllers, [1]. The other type of available digital devices for implementing industrial control systems is the Field Programmable Gate Arrays (FPGAs) technology, [6]. Most current FPGAs chips allow the implementation of efficient 32-bit processors. Therefore, FPGAs can be understood as programmable microcontrollers where application designers can combine one or several processors with dedicated peripherals and computing hardware accelerators, [7]. Both application components, hardware and software, must correctly interact in order to perform a given task. Those systems need a co-design approach and expertise to build a flexible embedded controller that can execute the real-time closed-loop control. The most common approach assuring high flexibility in designing an FPGA-based controller is interconnecting pre-designed hardware Intellectual Property (IP) blocks associated with the reconfigurable logic blocks and embedded software processors on the same chip, [8].

In this paper is presented the design approach and implementation of the control architectures for a hybrid renewable microgeneration prototype developed under the concept of a micro-grid. The power system contemplates two renewable energy sources (wind and solar), and a battery pack for energy storage. The three energy sources are individually controlled by different types of power electronics converters, using also different control solutions, allowing the optimization of each one individually. The system overview, at power level, is presented in Fig. 1.

Specific emphasis is given to the modelling and control of the AC-DC converters, one connecting the wind generator to the common DC-link bus and the other converter connecting the DC-link to the grid. They are more complex and are controlled using the same hardware/software design approach, based on an FPGA.

II. Grid Converter Control

The most used power electronic solution to connect different energy sources to the grid is composed by one voltage source converter (VSC) with a common DC-link. The DC-link voltage must be carefully regulated in order to have a robust and high efficiency system in terms of operation. Various control methods have been proposed to balance the power flow from the DC-link to the grid, [9]. The control methods can be classified as voltage-based ones, like direct power control (DPC) and voltage oriented control (VOC), as well as flux-based algorithms, inspired by motor control methods, like virtual flux oriented control (VFOC) and virtual flux-DPC (VF-DPC). In voltage oriented control methods the VSC is modeled as an AC voltage-controlled source. The converter is connected to the grid via a line impedance (usually a single inductance, L, with parasitic elements, R, although it can also be an LCL filter) as seen in Fig. 2. If the voltage source is controlled both in amplitude and phase, the active or reactive

978-1-5090-3474-1/16/$31.00 ©2016 IEEE

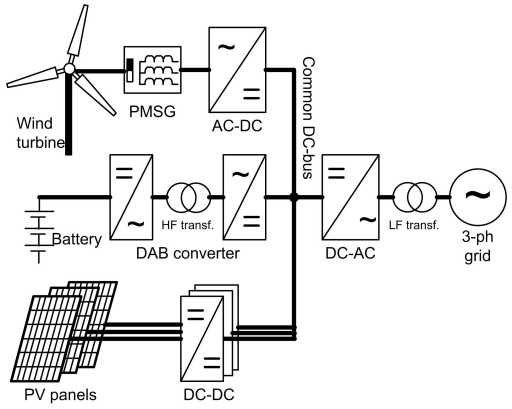

Fig. 1. Main architecture of the microgeneration system.

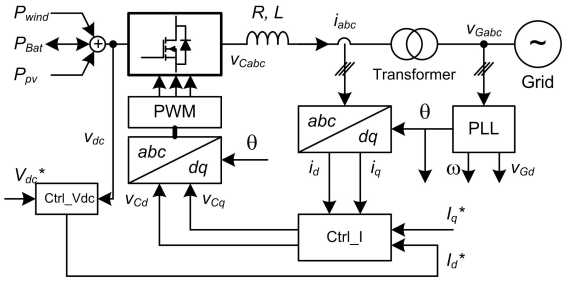

Fig. 2. VOC control method including the synchronization system, the current controller and the DC-bus voltage controller.

power flow to the grid is modified, [9]. Referring to Fig. 2, and assuming a balanced grid connection, the three-phase converter voltages are fully defined by (1):

$$[v_{Cabc}] = R[i_{abc}] + L\frac{d[i_{abc}]}{dt} + [v_{Gabc}] \tag{1}$$

The VOC method is based on a coordinate transformation between the stationary three-phase axes abc and the synchronous rotating dq reference frames. The relationship in (1) can be obtained in the dq reference frame using the Clarke-Park transformation, giving origin to (2):

$$\begin{cases} v_{Cd} = Ri_d + L\dfrac{di_d}{dt} + \omega L i_q + v_{Gd} \\ v_{Cq} = Ri_q + L\dfrac{di_d}{dt} - \omega L i_d + v_{Gq} \end{cases} \tag{2}$$

In (2), ω is the grid voltage angular frequency, estimated by means of a Phase-Locked Loop (PLL), v_{Gd} and v_{Gq} are the grid dq voltages, being v_{Gq} made zero by the synchronization method. The VOC scheme, shown in Fig. 2, is characterized by having three control loops to control the grid power flow through the VSC to the DC-link. Since the current control loops are decoupled, active (i_d) and reactive (i_q) components are independently controlled. In order to satisfy the imposed current set-points, I_d^* and I_q^*, the respective controllers change the VSC output voltage in order to reach the reference, [9].

The DC-link voltage is regulated imposing a reference in the active current component (I_d^*). A voltage variation in the DC-link is compensated by changing the AC active current in such a way that the DC-link is kept at the established value. The analysed system is a low-power one and so it is pretended to produce only active power; thus the reactive power current reference is imposed to be 0 A; however the control system is designed to accommodate a variable reactive current reference (I_q^*) in order to demonstrate the provision of grid services (reactive power control according to demanded set-points). In a different perspective, and depending on the active and reactive power supplied to the grid, the DC-link voltage reference can vary, thus achieving lower losses.

A. Grid Synchronization

Under balanced three phase systems, the most common and reliable state of the art PLL is the synchronous reference frame PLL (SRF-PLL), [10]. The SFR-PLL is a feedback control system that adjusts an internal generated signal (θ_g) in order to align the rotating dq frame with the grid phase, in such a way that cancels the grid reactive component (V_{Gq}). Once cancelled, the PLL architecture determines the amplitude (V_{Gq}), phase angle (θ_g), and frequency of the dominant component of an input signal (ω_g). The PLL used is the conventional one and consists of three basic functional blocks: phase detector, a low-pass filter and voltage controlled oscillator.

B. Current Controller

As shown in (2), the voltage control loops are decoupled, meaning that variations in one component do not perturb the other. Considering the decoupling terms, and according to (2), a PI controller is an appropriate one to control i_d and i_q; then the applied voltage components, v_{Cdq}, are given by (3):

$$\begin{cases} v_{Cd} = PI_d + \omega L i_q + v_{Gd} \\ v_{Cq} = PI_q - \omega L i_d \end{cases} \tag{3}$$

C. DC-link Voltage Controller

The DC-link is modelled as a pure capacitor. The capacitor is an energy storage device and the time derivative of the stored energy must be equal to the difference between the power from all sources connected to the DC-bus and the one injected into the grid, P_{dc}, as in Fig. 2 and (4):

$$\frac{dE_c}{dt} = \frac{1}{2}C\frac{dv_{dc}^2}{dt} = \sum_i P_i - P_{dc} \tag{4}$$

where P_i accounts for wind, battery and photovoltaic power and P_{dc} is the grid injected power. The DC voltage dynamics is non-linear with respect to v_{dc}. For an accurate control model, a linearisation of (4) was made, replacing v_{dc}^2 by W, and substituting P_{dc} by its AC equivalent, resulting in (5):

$$\frac{1}{2}C\frac{dW}{dt} = \sum_i P_i - \sqrt{3}V_{gLL}i_d \tag{5}$$

The process model, $G_v(s)$, is thus given by (6), acting the sum of the different energy sources as a global disturbance:

TABLE I
GRID SIDE CONVERTER PARAMETERS.

Symbol	Parameter	Rating
P_n	Nominal power	7.5 kW
V_{gLL}	Grid line-line voltage	400 V
a	Transformer ratio (V_{pri}/V_{sec})	2
L	Grid inductance	3.8 mH, R=0.1 Ω
V_{dc}	DC-link voltage	350-400 V
C_{dc}	DC-link capacitance	2 mF

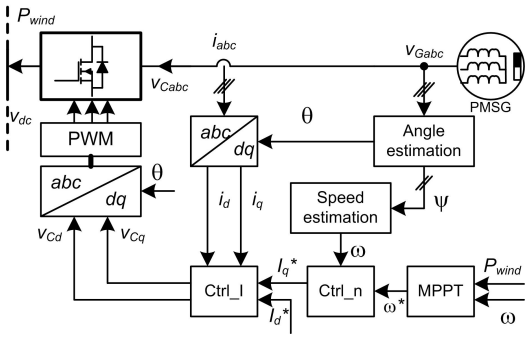

Fig. 3. Sensor-less voltage-oriented control of a PMSG-based wind generator.

$$G_v(s) = \frac{W(s)}{I_d(s)} = -\frac{2\sqrt{3}V_{gLL}}{sC} \tag{6}$$

As with the current controllers, a PI controller can accurately control the DC-link voltage. Its parameters were calculated in such a way that the DC voltage compensation has a fastest response to the reference and perturbations ($\sum P_i$). In order to evaluate the dynamics of the DC-link voltage, it was considered that the inductor value has a small value and so, the variations in the reactive current component caused by the DC voltage fluctuations were neglected. The system parameters used to design the controllers are presented in Table I.

III. WIND POWER CONVERTER CONTROL

Similar to the grid interfacing, a three-phase AC-DC converter is proposed for wind energy harvesting. The power flow is done from the wind generator through a Permanent Magnet Synchronous Generator (PMSG) to the common DC-link, being interfaced by one voltage source converter. The power flow must be regulated in order to achieve high level of robustness as well as extract the maximum power according to the wind operation conditions. This robustness level is supported by a current controller that operates in the active and reactive current components. The maximum power is obtained with a speed controller (Ctrl_n) and a Maximum Power Point Tracking (MPPT) controller that provides the optimum operational references for the current controller (Ctrl_I), according to Fig. 3. The position (θ) and frequency (ω) references are estimated through a sensor-less algorithm.

As with the grid converter, decoupled control of active and reactive power flow on the PMSG generator requires a synchronous coordinate transformation using the flux vector position. With the objective of avoiding the use of sensors, a complete sensor-less approach was assumed, both for the rotor position information and for the wind speed measurement.

A. Speed and Position Estimation

The rotor position estimation is based on the active flux concept. The two-phase stator flux estimation, using a fixed abc to $\alpha\beta$ coordinate transformation is given by (7), [11], where R_s, L_d and L_q are stator parameters:

$$\begin{cases} \psi_{d\alpha} = \int(u_\alpha - R_s i_\alpha)dt - L_q i_\alpha \\ \psi_{d\beta} = \int(u_\beta - R_s i_\beta)dt - L_q i_\beta \end{cases} \tag{7}$$

Therefore, the flux could be estimated for a wind generator using the same approach of PMSM with the voltage acquisition during the low speed operation and internal voltage references among with the two-phase reference frame stator currents for full speed operation of the PMSG. A modified integrator was used to avoid integrator saturation and DC bias problems. The position estimation is obtained with the four-quadrant $atan$ function, as given by (8):

$$\theta_r = \arctan\left(\frac{\int(u_\beta - R_s i_\beta)dt - L_q i_\beta}{\int(u_\alpha - R_s i_\alpha)dt - L_q i_\alpha}\right) \tag{8}$$

The rotor frequency estimation, required for appropriate decoupled control, is given by the frequency calculation from discrete time signals, as proposed in [12]. Being the estimated two-phase reference flux almost sinusoidal and given by a fixed sampling frequency, the two estimated flux references may be used to obtain the rotor frequency using (9):

$$f \cong \frac{1}{\pi T}\frac{(x_2[n]+x_2[n-1])x_1^{'}[n] - (x_1[n]+x_1[n-1])x_2^{'}[n]}{(x_1[n]+x_1[n-1])^2 + (x_2[n]+x_2[n-1])^2} \tag{9}$$

where $x_1[n]$ and $x_2[n]$ are the estimated fluxes in β and α axes, respectively, $x_1[n-1]$ and $x_2[n-1]$ are the estimated fluxes in the previous code execution in β and α axes, respectively. Also, $x_1^{'}[n]$ and $x_2^{'}[n]$ are the β and α frame derivatives and are given by the following equation (backward difference):

$$x^{'}[n] = \frac{x[n] - x[n-1]}{\Delta T} \tag{10}$$

B. Current Controller Design

Similarly to the grid interfacing converter, the wind generator has the voltage control loops decoupled. The current control follows the control strategy proposed by [13], where the voltage references in rotating dq frames are obtained by the decoupling either of the active current influence in reactive frame and vice-versa. Thus, the PMSG model is obtained in the dq reference frame in a similar mode, where ω is the electrical rotating speed:

$$\begin{cases} v_{Cd} = -R_s i_d - L_d\dfrac{di_d}{dt} - \omega L_q i_q + v_{Gd} \\ v_{Cq} = -R_s i_q - L_q\dfrac{di_q}{dt} + \omega L_d i_d + v_{Gq} \end{cases} \tag{11}$$

In the case of the PMSG control, v_{Gd} is chosen to be zero, and each i_d and i_q synchronous reference currents are controlled individually through a PI controller. The output of direct (d) component of PI is added to the decoupling component accordingly to (12) obtaining the direct synchronous reference of voltage:

$$\begin{cases} v_{Cd} = -PI_d - \omega L_q i_{sq} \\ v_{Cq} = -PI_q + \omega L_d i_{sd} + \omega \psi_r \end{cases} \quad (12)$$

In the same decoupling strategy, the synchronous quadrature reference of the voltage is obtained by adding the decoupling component in (12) to the PI quadrature reference. Voltages v_{Cd} and v_{Cq} are then converted to the three-phase frame reference and the sinusoidal pulse width modulation (SPWM) method is applied to the VSC using those references. The SPWM frequency is 20 kHz. The position and speed estimation and the current controller are executed in the same control layer at 5 kHz frequency (1/Tc1 in Fig. 7a)).

C. Speed and MPPT Controllers

In a different control layer, the speed and MPPT controllers are executed in a parallel execution architecture. A different execution frequency is then proposed. The MPPT controller uses the angular speed of the generator and the active power to generate incremental references to the speed controller at 100 Hz execution frequency (1/Tc3 in Fig. 7a)). The speed controller is executed at 1 kHz (1/Tc2 in Fig. 7a)), and, through an anti-windup PI controller, provides an active current reference to the current controller (with $I_d^* = 0$, for non-additional magnetization).

IV. Control, Monitoring and Communications

A hierarchical layered approach was designed for the control, monitoring/supervision and remote access processes. This global architecture is shown in Fig. 4. The adoption of Raspberry Pi platforms on Internet of Things (IoT) has become a common practice among researchers and solution providers, [14]. Claiming the production of 8 million units in all distributions, the attributes of cost effective, versatile and uncomplicated platforms for rapid application development as well as the high amount of reported solutions in the Internet with the successful use of this platform are the main reasons to support this adoption.

A second generation of Raspberry Pi is proposed for data monitor managing and system supervision of this micro-generation system. This CPU uses the official "Raspbian" Operating System (OS), based in Linux Debian kernel, but developed for this platform. The software is implemented in Qt Integrated Development Environment (IDE) which allows the use of C++ language and several available libraries. This OS has also a web server running a PHP script for data presentation on a web page and a relational database holding the overall system data.

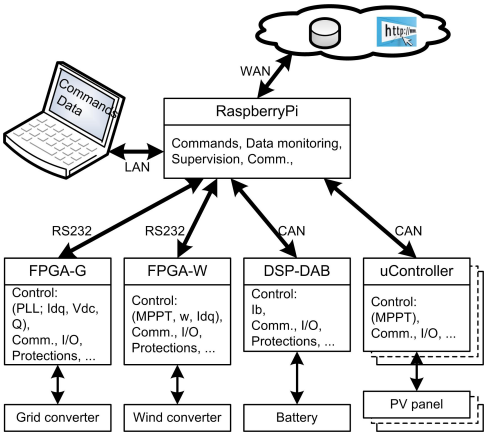

Fig. 4. Overview of all control and communication services included in the global renewable energy system.

A. Software Layers

The software layers are divided into Power-On, Acquisition, Processing, Updating and Data Logging. Power-on is running each time the system starts. It has to configure every connection between this top layer and the low level peripherals, as well as setting-up the relational database interaction. Acquisition layer collects every data from lower level as well as manages the synchronization of each acquired data. Processing executes the supervision on lower peripherals as well as data analysis for power flow reference generator. Updating is responsible for sending the processed data to low level peripherals. Data Logging manage to send the acquired and processed variables to a database for future analysis and website data updating.

B. Communications Protocols

The communications are hardware implemented through an USB-RS232 transceiver for FPGA interface and through an USB-CAN transceiver implemented with an Arduino Uno device and a CAN shield. The FPGA has implemented a question-answer transaction protocol with a check-sum error correction implemented. This device is also available for receiving sync commands for sampling and hold the current variables and, in the FPGA controlling the grid converter, this protocol has the availability to receive the DC-link voltage and reactive current references. The Arduino Uno device has the same protocol implemented and is also responsible for managing the data exchange between the CAN bus where the battery charger DSP peripheral is connected. Current reference for the battery is received by Arduino that follows this reference through the CAN bus. Finally, all PV modules are connected to a common CAN bus and, similarly to battery charger, an Arduino Uno device coupled to a CAN shield is responsible to interface the variables being exchanged in CAN bus to the Raspberry Pi through the USB.

C. State Machines

The two addressed converters manage energy levels requiring tight control, safety and flexible operation. Therefore, state

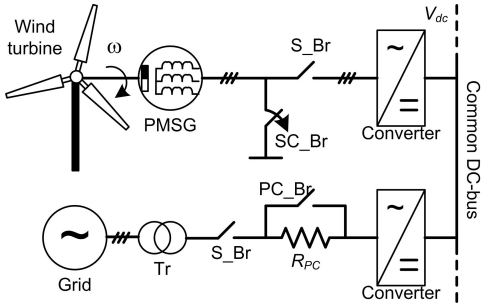

Fig. 5. Diagram of main circuit breakers in the two FPGA-based controlled converters.

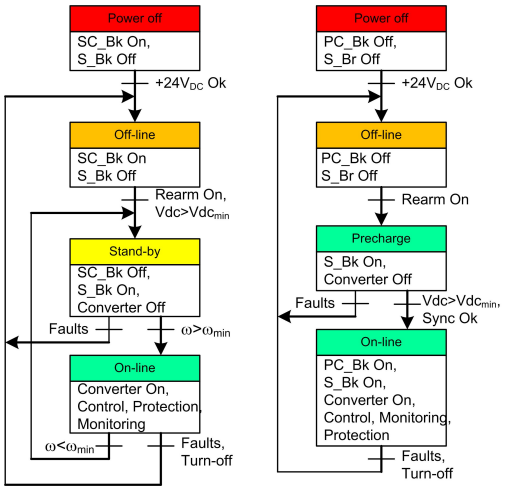

Fig. 6. State machines for the two converters: wind converter (left) and grid converter (right).

machines are in the top-level of their control and command functions. Safety operation for both converters is achieved by means of manual switches (not shown) and controlled circuit breakers, according to the diagram in Fig. 5 S_Br are series breakers (normally open), SC_Br is a short-circuit parallel breaker (normally closed), and PC_Br is a pre-charge breaker (normally open).

The detailed state machines for the two converters, shown in the diagram in Fig. 6, including the main operation controls and conditions, will be further described in Section V.

V. FPGA-Based Implementation

The development strategy is focused on developing Intellectual Property (IP) cores as key building blocks for data exchange. The layering strategy is used either for the grid interface FPGA and the wind harvesting one; Fig. 7 shows the approach for the two converters, based on the defined soft processors (MicroBlaze-uB). For the wind converter, uB1 executes the tasks related to the rotor position estimation, using a discrete version of (8), speed estimation, (9), and current control, (12), while uB2 executes the MPPT and the speed control tasks. The basic hardware (external and internal to the FPGA board) supporting the control functions is represented in Fig. 8 for the wind power converter.

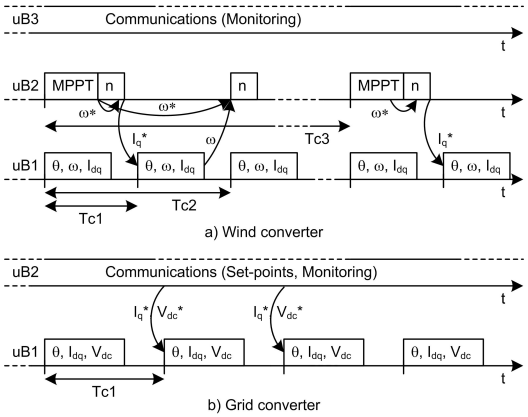

Fig. 7. Control flow strategy for the two converters: a) wind converter and b) grid converter.

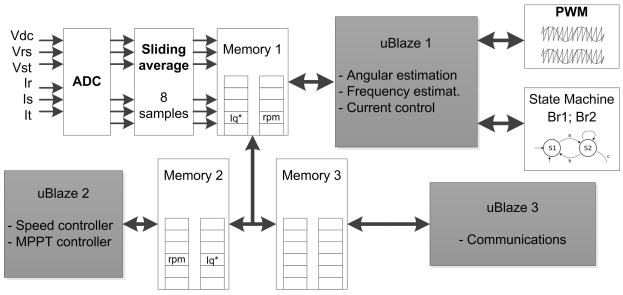

Fig. 8. Wind converter hardware and software control implementation.

Due to the algorithm execution time restrictions, the wind harvesting FPGA needs parallel execution for lower timing algorithms while the grid converter lower execution time algorithm (DC-bus voltage controller) is able to do it without parallel execution needs. Therefore, there is no need of usage of uBlaze2 for DC-bus voltage controller being this controller executed in the main controller (uBlaze1). The data acquisition is done by one differential ADC per each channel allowing up to 500 kHz of data acquisition for each input. A 200 kHz rate was chosen for each ADC update and the data acquisition is updated in this IP core at 40 kHz rate. A sliding average IP core of 8 samples was proposed for signal conditioning before the data is stored in a memory IP core. This memory block also allows the data exchange between different processing units (uBlaze soft CPU). In both FPGAs, the main control unit, uBlaze1, estimates the angle/position and frequency of the system (rotor or frequency of the grid) and generates the three phase voltage references from the current controller algorithm. This control unit also generates the transition references for the state machine. From the output side, there is the PWM IP core that generates the PWM references at 20 kHz switching frequency for each transistor, with a specific dead-time for the transistor transitions of the same branch.

There is also the State Machine IP core that is responsible for the enabling and disabling of the outputs, namely the power breakers and the PWM. In wind harvesting FPGA the states

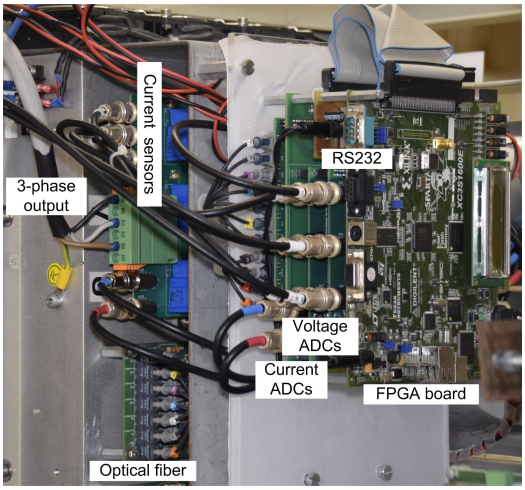

Fig. 9. Hardware platform associated with the grid converter.

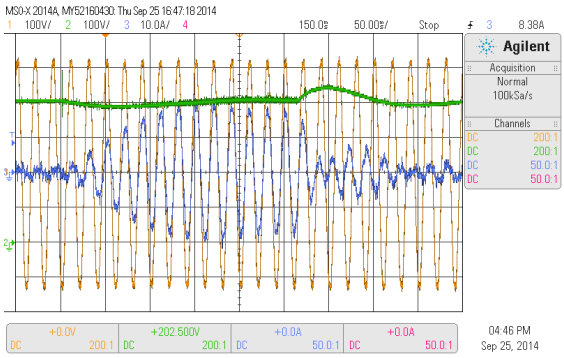

Fig. 10. Grid converter transient and steady-state operation. Channels: yellow: line-neutral phase a voltage (100 V/div); blue: phase a current (10 A/div); green: DC voltage (100 V/div). Time: 50 ms/div.

are associated to the speed of the wind turbine and, in normal operation, those states alternate between Stand-by and On-line, depending on the existence of enough wind to generate energy. In grid interface FPGA there is a need to charge the DC-bus in power-on of this system before it enters in normal operation. From on-line state, the current and voltage controllers are able to fix the DC-bus voltage accordingly to a reference provided by the top level. The secondary control units generate the current references for the main controller and manage the communications with top level, respectively through uBlaze2 and uBlaze3 soft CPU's. Those timings are represented on Fig. 7.

A. Prototype and Results

A partial view of the FPGA board controlling the grid converter, including several peripherals, is shown in Fig. 9.

In Fig. 10, the three controllers inside the grid converter are in good operation: the AC current is synchronized with the grid voltage; the reactive current is regulated to zero and the DC voltage is correctly controlled under soft-start and sudden interruption of active power flow.

VI. Conclusion

An FPGA-based HW/SW architecture for controlling two PWM converters inside a hybrid renewable micro-generation system (wind and solar, storage battery and connection to the grid), was presented. The main models related to control, monitoring and communications tasks were discussed and evaluated. The experimental platform and results support the approach and demonstrate the appropriateness of the FPGA-based solutions to control demanding systems both in real-time requirements and in the complex controllers.

Acknowledgment

This work was financially supported by: Project POCI-01-0145-FEDER-006933 - SYSTEC - Research Center for Systems and Technologies.

References

[1] C. Buccella, C. Cecati, H. Latafat, "Digital control of power converters-a survey", *IEEE Tr. on Industrial Informatics*, vol. 8, no. 3, pp. 437-447, Aug. 2012.

[2] T. Atalik, M. Deniz, E. Ko, C. . Gerek, B. Gltekin, M. Ermis, I. adirci, "Multi-DSP and -FPGA-based fully digital control system for cascaded multilevel converters used in FACTS applications", *IEEE Tr. on Industrial Informatics*, vol. 8, no. 3, pp. 511-527, Aug. 2012.

[3] Altera, "FPGA-based control for electric vehicle and hybrid electric vehicle power electronics", Altera Corporation, White paper, pp. 1-24, Dec. 2013.

[4] E. J. Bueno, Á. Hernández, F. J. Rodríguez, C. Girón, R. Mateos, S. Cóbreces, "A DSP- and FPGA-based industrial control with high-speed communication interfaces for grid converters applied to distributed power generation systems", *IEEE Tr. on Industrial Electronics*, vol. 56, no. 3, pp. 654-669, March 2009.

[5] S. Buso, T. Caldognetto, "Rapid prototyping of digital controllers for microgrid inverters", *IEEE Tr. on Emerging and Selected Topics in Power Electronics*, vol. 3, no. 2 pp. 440-450, June 2015.

[6] E. Monmasson, L. Idkhajine, M. N. Cirstea, I. Bahri, A. Tisan, M. W. Naouar, "FPGAs in industrial control applications", *IEEE Tr.on Industrial Informatics*, vol. 7, no. 2, pp. 224-243, May 2011.

[7] A. K. Salem, S. B. Othman, S. B. Saoud, "Field programmable gate array-based system-on-chip for real-time power process control", *American Journal of Applied Sciences*, vol. 7, no. 1, pp. 127-139, 2010.

[8] P. Garcia, K. Compton, M. Schulte, E. Blem, W. Fu, "An overview of reconfigurable hardware in embedded systems", *EURASIP Journal on Embedded Systems*, vol. 2006, pp. 1-19.

[9] J. Rodríguez, J. Dixon, J. Espinoza, J. Pontt, and P. Lezana, "PWM regenerative rectifiers: state of the art", *IEEE Tr. on Industrial Electronics*, vol. 52, no. 1, pp. 5-22, Feb. 2005.

[10] F. Blaabjerg, R. Teodorescu, M. Liserre, A. Timbus, "Overview of control and grid synchronization for distributed power generation systems", *IEEE Tr. on Industrial Electronics*, vol. 53, no.5, pp.1398-409, Oct. 2006.

[11] Q. Yuan, Z. Yang, F. Lin, H. Sun, "Sensorless control of permanent magnet synchronous motor with stator flux estimation", *Journal of Computers*, vol. 8, no. 1, pp. 108-112, Jan. 2013.

[12] P. J. Moore, R. D. Carranza, A. T. Johns, "A new numeric technique for high-speed evaluation of power system frequency", *IEE Proc.-Gener. Transm. Distrib.*, vol. 141, no. 5, pp. 529-536, Sept. 1994.

[13] J. S. Thongam, R. Beguenane, M. Tarbouchi, A. F. Okou, A. Merabet, I. Fofana, P. Bouchard, "A rotor speed estimation algorithm in variable speed permanent magnet synchronous generator wind energy conversion system", *Int. J. Robust Nonlinear Control*, vol. 23, pp. 1880-1890, 2013.

[14] C. P. Kruger, G. P. Hancke, "Benchmarking internet of things devices", in *Proceedings of the 12th IEEE Int. Conf. on Industrial Informatics* (INDIN), 27-30 July 2014, Porto Alegre, Brazil, 611-616, 2014.